

# Analyzing the influence of particle size and stiffness state of the nanofiller on the mechanical properties of epoxy/clay nanocomposites using a novel shear-stiff nano-mica

Martin Heinz Kothmann<sup>1</sup> · Mazen Ziadeh<sup>2</sup> · Gökhan Bakis<sup>1</sup> · Agustin Rios de Anda<sup>1,3</sup> · Josef Breu<sup>2</sup> · Volker Altstädt<sup>1</sup>

Received: 19 January 2015 / Accepted: 15 April 2015 / Published online: 1 May 2015  
© Springer Science+Business Media New York 2015

**Abstract** The mechanical properties of epoxy/clay nanocomposites were investigated in relation to the particle size and shear stiffness state of the dispersed nanoplatelets. The fracture toughness and the underlying toughening mechanisms were thoroughly discussed in detail. For this study, a highly pure synthetic fluorohectorite with large lateral extensions ( $\approx 3.8 \mu\text{m}$ ) was used and compared to natural montmorillonite characterized by significantly smaller lateral extensions ( $\approx 400 \text{ nm}$ ). Moreover, for the synthetic fluorohectorite, the subtle balance between layer charge density and the hydration enthalpy of interlayer cations allows for switching between a shear-labile and

shear-stiff state, something impossible for the natural material. To ensure optimum dispersion, solution blending was followed by three roll milling for nanocomposite preparation. The addition of all three types of clay used in this study provoked a decrease in glass transition temperature, which indicated a moderate interfacial strength. The maximum increase in fracture toughness and strain energy release rate was observed for the nanocomposites prepared with the large and shear-stiff fluorohectorites at a particle content as low as 2.2 vol%. Morphological investigations by scanning electron microscopy of the fracture surfaces revealed the contribution of several micro-mechanical toughening mechanisms. In contrast to the small natural montmorillonite, the large synthetic nanoplatelets promoted additional energy dissipating mechanisms such as crack deflection and crack pinning leading to an enhanced fracture toughness. These observations are discussed in details using fracture mechanical approaches.

Martin Heinz Kothmann and Mazen Ziadeh have contributed equally to this work.

✉ Volker Altstädt  
altstaedt@uni-bayreuth.de

Martin Heinz Kothmann  
martin.kothmann@uni-bayreuth.de

Mazen Ziadeh  
mazen.ziadeh@uni-bayreuth.de

Gökhan Bakis  
goekhan.bakis@uni-bayreuth.de

Agustin Rios de Anda  
agustin.riosdeanda@cermav.cnrs.fr

Josef Breu  
josef.breu@uni-bayreuth.de

<sup>1</sup> Lehrstuhl für Polymere Werkstoffe, Universität Bayreuth, 95440 Bayreuth, Germany

<sup>2</sup> Lehrstuhl für Anorganische Chemie I, Universität Bayreuth, 95440 Bayreuth, Germany

<sup>3</sup> Present Address: Centre de Recherche sur les Macromolécules Végétales (CERMAV), UPR 5301 CNRS, Saint Martin d'Hères, France

## Introduction

Epoxy resins are widely employed in various industrial applications, which range from protective coatings to matrices in structural fiber-reinforced composites for diverse automotive and aviation components. Despite having several advantages in terms of processing and mechanical properties, epoxy systems suffer from high brittleness due to the densely cross-linked network structure. Many attempts to improve the inherently low fracture toughness were carried out either by decreasing the network density [1] or introducing rubber-based toughening agents [2]. Nevertheless, in most cases, the toughening of epoxy resins was accompanied by a decline of both the elastic modulus

and the glass transition temperature [2, 3]. In contrast to these approaches, incorporating inorganic nano-particles into the epoxy matrix provided a suitable solution to overcome the low toughness without sacrificing the inherent matrix properties (i.e., strength). For instance, the incorporation of spherical nano-silica (diameter  $\approx 20$  nm) led to a nearly two-fold improvement in toughness and elastic modulus at 15.1 vol% particle content [4]. However, high filler contents are required to achieve such enhancements. In order to obtain a further improvement in toughness and stiffness simultaneously, the use of platelet-like nano-particles is favorable [5–7]. These nano-particles provide a significantly larger lateral expansion in addition to a high in-plane modulus, which can be transferred to the matrix by an optimum interfacial adhesion [8–10].

Among the plethora of platelet-like nano-particles, the layered silicates of the smectite family (e.g., natural montmorillonite—MMT) emerge as suitable nanofillers after an organophilization process. In order to improve the compatibility of the hydrophilic layered silicates in the polymeric matrix, the surface tension can be lowered by a simple cation exchange with organic molecules. Most commonly, alkyl-ammonium cations with various chain lengths are used for organophilization [11]. For instance, organo-modified MMT-filled epoxy nanocomposites showed significant improvements in toughness (60 %) at 5 wt% clay content, though less pronounced improvements in modulus (10 %) were achieved [12]. In many cases, optimum dispersion of MMT tactoids was not achieved, instead micron-sized aggregates were spotted. These aggregates may be attributed to associated impurities and amorphous materials such as iron- and aluminum-oxihydroxides in natural MMT deposits acting as binders [13]. Therefore, such natural fillers are difficult to be disaggregated and even more to be completely delaminated [14]. Furthermore, due to their genesis, the charge density in natural clays is heterogeneous, leading to a non-uniform surface chemistry hindering the adjustment of the stiffness state.

Synthetic layered silicates can be considered as suitable candidate materials to overcome these drawbacks due to their high purity and homogenous layer charge density. Although a better and more homogeneous dispersion was achieved, the improvements in toughness and/or stiffness of such systems were comparable to natural MMT/nanocomposites [5, 15]. The moderate fracture toughness was related to proposed length-scale argument by Kinloch and Taylor [7]. It was suggested that a minimum particle size is required to promote on-plane toughening mechanisms (i.e., crack pinning and deflection) by effective crack/particle interactions. In this context, the addition of 5 wt% non-modified mica, characterized by a large lateral extension (50  $\mu\text{m}$ ), increased the fracture

toughness two-fold alongside a moderate improvement in modulus by 20 % [7].

Considering the upper mentioned length-scale argument, the aim of the present study is to understand and quantify the effect of particle size and shear stiffness on the toughening of epoxy resins using different clay materials and even more to evaluate the underlying toughening mechanisms with respect to the particle size. To achieve this aim systematically, as a common reference material, natural montmorillonite characterized by a small lateral extension (ca. 0.4  $\mu\text{m}$ ) with lower shear stiffness (hydrated interlayer structure, named shear-labile) is used. Alongside, synthetic fluorohectorites having bigger lateral extensions (ca. 3.8  $\mu\text{m}$ ) with lower (with hydrated interlayers, named shear-labile) and higher shear stiffness states (collapsed non-hydrated interlayers, named shear-stiff) were prepared and used. A synthetic Na-fluorohectorite prepared in a melt synthesis is applied. This filler is characterized by large lateral extensions (ca. 3.8  $\mu\text{m}$ ) and outstanding layer charge homogeneity. The homogenous charge density allows for a transformation between highly hydrated shear-labile (lower shear stiffness) and a non-hydrated shear-stiff state (higher shear stiffness) by simple cation exchange. Due to its inhomogeneous layer charge density and amorphous impurities this transformation is not possible for common natural MMT [16–18]. Consequently, the influence of stiffness state of the nanofiller on the mechanical properties of the epoxy/clay nanocomposites was analyzed in detail using the shear-stiff K-hectorite (O/K-hect) and the shear-labile (O/Mg-hect).

These three types of layered silicates allow a systematic investigation on the impact of the dispersed filler, in terms of lateral extension and stiffness state—labile or stiff—on the mechanical properties, especially the fracture toughness of the epoxy nanocomposites and the underlying toughening mechanisms.

As a prerequisite to analyze the gained results, a homogenous dispersion, alongside the knowledge of the particle size, is essential. For this reason, the strategy of particle modification and dispersion is described in detail. Furthermore, the results of the particle size analysis via static light scattering (SLS) are presented in detail.

## Experimental

### Materials

Synthetic Na-fluorohectorite was prepared by melt synthesis with an idealized chemical formula of  $\text{Na}_{0.5}[\text{Mg}_{2.5}\text{Li}_{0.5}\text{Si}_4\text{O}_{10}\text{F}_2]$ . The cation exchange capacity (CEC) was determined to be 110 meq./100 g using the copper complex method [19]. As described in the following, the

Na-fluorohectorite was used to prepare the shear-labile Mg-fluorohectorite (Mg-hect) and the shear-stiff K-fluorohectorite (K-hect) by cation exchange reactions.

As a smectite clay reference, natural MMT supplied by Nanocor<sup>®</sup> (Illinois, USA) was employed. The clay has a reported CEC of 125 meq./100 g, however, it was found to be only 90 meq./100 g as determined by the copper complex method.

Dodecylamine (97 %, Sigma-Aldrich) was used for the organophilization of the hydrophilic layered silicates after protonation with an equimolar of HCl (0.1 M). Magnesium chloride (hydrated) and Potassium chloride were used for cation exchange reactions (Grüssing GmbH Analytika). Analytical grade tetrahydrofuran (THF 99.9 %) and anhydrous ethanol (EtOH) were purchased from Sigma-Aldrich and used as received.

Diglycidylether of bisphenol A epoxy resin, EPIKOTE<sup>™</sup> Resin 0162 (Momentive Specialty Chemicals GmbH), and methylhexahydrophthalic acid anhydride curing agent, EPICURE<sup>™</sup> Curing Agent 868 (Momentive Specialty Chemicals GmbH), were purchased for the preparation of the epoxy network. *N,N'*-Dimethylbenzylamine (99 %, Sigma-Aldrich) was used to accelerate curing.

### Tailoring the nanofiller properties

#### *Maximization of aspect ratio and rendering the stiffness state*

In order to prepare the shear-labile Mg-fluorohectorite (Mg-hect) and the shear-stiff K-fluorohectorite (K-hect), the synthetic Na-fluorohectorite was, as an initial step, transformed to a highly hydrated shear-labile state by a cation exchange of the interlayer Na<sup>+</sup> with Mg<sup>2+</sup> cations in an aqueous suspension [16–18]. This Mg-hect with its highly hydrated state in an aqueous dispersion was processed in a stirred media mill in order to exfoliate the nanofiller tactoids by applying mechanical shear forces. After milling, the typical tactoid thickness was found to be (10–15 nm) [18]. As a first approximation of the lateral extension, the hydrodynamic radius obtained from SLS is used [20].

Subsequent to the exfoliation process, half of the Mg-hect sample was exchanged with K<sup>+</sup> cations. After dehydration, the obtained K-hect is in a shear-stiff, mica-like state without intracrystalline reactivity [16]. In this collapsed state, the interlamellar space of K-hect is no longer accessible for organic molecules and the CEC value is attributed solely to the external basal planes of the tactoids. Consequently, the CEC value of K-hect was determined to just 18 meq./100 g using the copper complex method [19].

An overview of all processing steps starting with the synthesized Na-hect is schematically shown in Fig. 1a.

### *Organophilization of nanofillers*

A standard procedure for organophilization was employed for all three types of nanofillers (MMT, Mg-hect, and K-hect). Cation exchange was carried with the amounts of dodecylammonium chloride corresponding to the CEC of each nanofiller [21]. First an aqueous solution of dodecylammonium chloride was added slowly to an aqueous suspension of the clay. The modification triggered flocculation of the nanoplatelets in the aqueous suspension. These flocculated nanoplatelets were centrifuged and washed with a mixture of ethanol/water (1:1<sub>vol</sub>) and subsequently phase transferred into THF (Fig. 1b). The three employed nanofillers and their specific properties are given in Table 1. In order to distinguish the organophilized nanofillers, they are further referred with a prefixed O (O/MMT, O/Mg-hect, and O/K-hect).

### Preparation of epoxy/clay nanocomposites

For each type of nanofiller, a series of nanocomposites with various clay contents (1.25, 2.5 and 5.0 wt%) were prepared. In order to explain the observed phenomena, the weight fraction is converted to volume fraction, considering the real filler content determined by thermogravimetric analyses and the filler density.

As a general procedure for all three types of clay, after organophilization, the nanofiller/THF suspension was mixed with the dissolved epoxy resin by stirring it in a round flask for 1 h. Then the solvent was removed in a rotary evaporator under vacuum at 80 °C (Fig. 1b). Subsequently, the anhydride hardener was added to the epoxy-nanofiller mixture according to its stoichiometric ratio. The final mixture (epoxy, hardener, and nanofiller) was processed using a EXAKT E80 three roll mill (Exakt Vertriebs GmbH) to achieve an optimal dispersion prior to curing. The mixture was fed directly to the first roll and sheared between the gaps, after which the dispersion was repeatedly fed into the machine for the next passage (Fig. 1c). During the dispersing process, the adjacent rollers rotate at different speeds and in counter rotational directions. A rotational speed of 300 min<sup>-1</sup> was fixed and the gap sizes were set to provide an increase of the shear rates by a stepwise reduction of the gap width for each passage (Table 2). The particle size distribution was then determined after each passage using static light-scattering measurements.

Subsequently to the three roll mill process, 1 wt% of *N,N'*-Dimethylbenzylamine, as referred to the liquid matrix, was added to accelerate the curing process. The mixture was degassed under vacuum at 60 °C for 15 min and then cured at 140 °C for 11 h in an aluminum mold coated with release agent (Loctite Frekote 770-NC, Henkel AG & Co. KGaA) to produce 4-mm-thick nanocomposite plates.

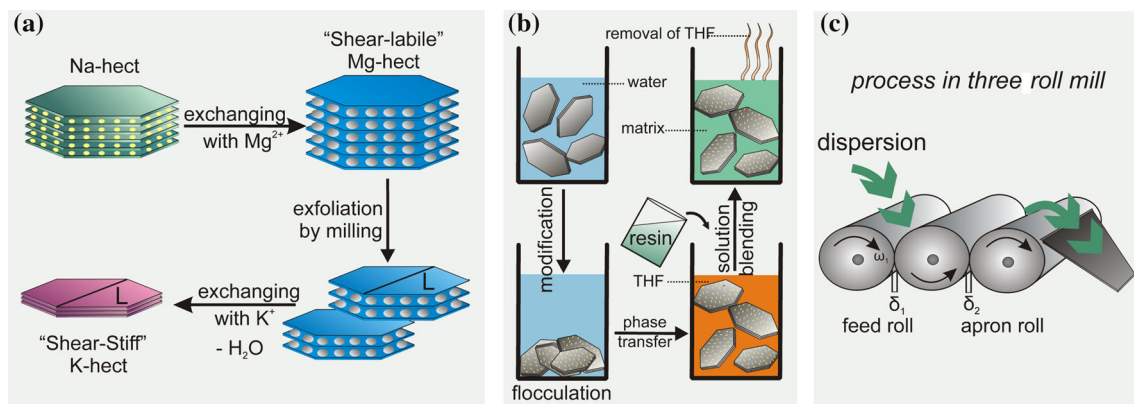


**Fig. 1** **a** Production of high aspect ratio shear-labile Mg-hect by exfoliation in a stirred media mill and its subsequent cation conversion into a non-swollen, shear-stiff nano-mica (K-hect) by cation exchange, **b** selective organophilization of external basal

planes of K-hect, phase transfer, and solution blending with the epoxy resin, and **c** dispersion of the nanofiller in the epoxy matrix using a three roll mill in a continuous operation

**Table 1** Nomenclature and properties of the three different employed organophilized nanofillers

Name of nanofiller	Mean lateral extension ( $\mu\text{m}$ )	CEC (meq./100 g)	State of shear stiffness	Modification sites
O/MMT	0.4	90	Labile	External and internal surfaces
O/Mg-hect	3.8	110	Labile	External and internal surfaces
O/K-hect	3.8	18	Stiff	Only external surfaces

**Table 2** Processing parameters of the three roll mill

	1st gap distance ( $\mu\text{m}$ )	2nd gap distance ( $\mu\text{m}$ )	Roll speed (rpm)
1st passage	30	20	300
2nd passage	20	15	300
3rd passage	15	10	300

## Characterization methods

Powder X-ray diffraction (PXRD) patterns were obtained using Nickel-filtered Cu-K $\alpha$  radiation ( $\lambda = 1.54187 \text{ \AA}$ ) on a Bragg–Brentano-type diffractometer (PANalytical XPERT-PRO, Spectris) equipped with an X'Celerator Scientific RTMS detector. Textured samples were prepared by the slow evaporation of clay suspensions in THF on planar glass slides. PXRD patterns of the final nanocomposites were obtained with powder samples obtained by grinding applying a pulverisette 14 cryo-grinder (Fritsch, 2 mm sieve). PXRD patterns for these samples were obtained in transmission geometry on a STOE Stadi P (Stoe & Cie) powder diffractometer equipped with a MYTHEN1 K detector using Cu K $\alpha_1$  radiation ( $\lambda = 1.54056 \text{ \AA}$ ).

The amount of organic content in the different organically modified nanofillers as well as the nanofiller content in the nanocomposites was determined by thermogravimetric analysis (TGA). The measurements were carried out using a TGA/STDA851e (Mettler Toledo). The nanofillers were heated up to 700 °C and the cured epoxy

nanocomposites up to 1100 °C under oxygen flow (50 ml/min) at a heating rate of 10 K/min.

The particle size distribution was recorded for suspensions of the nanofiller in THF (1 wt%) on a Horiba LA-950 static light-scattering instrument (Retsch Technology GmbH). The refractive indices for nanofiller and THF were chosen as 1.590 and 1.407, respectively.

The dispersion quality of the nanofiller in the epoxy matrix was monitored using a LEO 922 A EFTEM transmission electron microscope (Carl Zeiss AG), with an acceleration voltage of 200 kV. Thin sections of 50 nm were cut on a Leica Ultracut microtome (Leica Biosystems GmbH) equipped with a glass knife. Fracture surfaces of selected  $K_{1c}$  samples were analyzed using a Zeiss 1530 (Carl Zeiss AG) scanning electron microscope possessing a field emission cathode for high-resolution micrographs using an acceleration voltage of 1.5 kV.

Dynamical mechanical thermal analyses (DMTA) were performed according to DIN EN ISO 6721-7 using an Advanced Rheometric Expansion System (ARES RDAIII, Rheometrics Scientific) in torsional mode. A sinusoidal

deformation of 0.1 % with a frequency of 1 Hz was applied, from 25 to 200 °C at a heating rate of 3 K/min. According to the standard, rectangular samples were used (50 × 10 × 2 mm<sup>3</sup>). The glass transition temperature (*T<sub>g</sub>*) of the epoxy nanocomposites was determined as the maximum of the loss factor, tan δ.

Tensile tests were performed at 25 °C according to EN ISO 527-2 using a universal testing machine (Zwick 1475, Zwick GmbH & Co. KG) equipped with a 100 kN load cell. The longitudinal and lateral strains were measured by mechanical extensometers (BZ1-EXZW004, respectively, BZ1-EXZW014, Zwick GmbH & Co. KG). To determine the Young’s modulus, a crosshead speed of 1 mm/min was applied. For the tensile strength and the elongation at break, a crosshead speed of 5 mm/min was performed.

The fracture toughness, in terms of the critical stress intensity factor (*K<sub>Ic</sub>*), was determined according to ISO 13586 using CT specimens. The specimen width was *w* = 33 mm and the thickness was *d* = 4 mm. For each sample, a sharp crack was generated by tapping a new razorblade into the machined V-notch. The tests were carried out using a universal testing machine (Zwick BZ2.5/TN1S, Zwick GmbH & Co. KG). The crack opening displacement was measured using a clip extensometer (632.29F-30, MTS Sensor Technologie GmbH & Co. KG). The critical stress intensity factor was calculated using Eq. (1):

$$K_{Ic} = \frac{F_{max}}{d \cdot \sqrt{w}} \cdot f\left(\frac{a}{w}\right), \tag{1}$$

where *F<sub>max</sub>* represents the maximum force required for crack propagation, *a* is the initial crack length, and *f* (*a/w*) is a geometrical term defined in the ISO 13586. In addition, the critical energy release rates (*G<sub>Ic</sub>*) of the neat epoxy and the epoxy/clay nanocomposites were calculated according to Eq. (2):

$$G_{Ic} = \frac{K_{Ic}}{E} \cdot (1 - \nu^2), \tag{2}$$

where *E* is the Young’s modulus and *ν* the Poisson’s ratio of the nanocomposites as determined via tensile testing. In order to gain a better understanding of the apparent fracture toughening mechanisms, the diameter of the plastic zone in the vicinity of the crack tip is calculated from Eq. (3).

$$d_{Irwin} = \frac{1}{3\pi} \left( \frac{K_{Ic}}{\sigma_y} \right)^2. \tag{3}$$

Furthermore, the crack tip opening displacement (*δ<sub>Ic</sub>*) is calculated according to Irwin [22] (Eq. 4) using the data of the tensile and fracture toughness tests.

$$\delta_{Ic} = \frac{K_{Ic}^2}{E \cdot \sigma_y} (1 - \nu^2). \tag{4}$$

Plane strain conditions were assumed for all calculations.

## Results and discussion

### Preparation and characterization of the organophilized nanofillers

In this chapter, the main results regarding the production and exfoliation of the synthetic fluorohectorite are presented. Moreover, the organophilization process is analyzed thoroughly in terms of organic content and intergallery distance of the modified clays.

As described in detail by Möller et al. [16], the synthetic Na-hect allows a controlled transformation between a highly hydrated shear-labile and a non-hydrated shear-stiff state by a simple cation exchange of the interlayer Na<sup>+</sup> cations with Mg<sup>2+</sup> (Mg-hect), respectively, K<sup>+</sup> (K-hect). This transformation is enabled by the subtle balance between layer charge density and the hydration enthalpy of the different interlayer cations in the synthetic clay [16]. On the contrary due to its lower and more heterogeneous layer charge density this transition between hydration states is not feasible for natural MMT. In the shear-stiff K-hect, the interlayer space is no longer accessible neither for hydration nor for cation exchange after collapsing and therefore organophilization is restricted to external basal planes [16].

Organophilization achieved by modification of the external basal surfaces via cation exchange mainly serves two purposes. On the one hand, the surface tension is lowered in order to achieve a good dispersion of the nanofiller in polymer matrix. On the other hand, the matrix-nanofiller interaction is improved relative to the filler–filler interaction. By this, the load transfer at the interface is enhanced and aggregation is minimized. Formation of aggregates will of course reduce the specific interface area in the nanocomposite and consequently will hamper potential improvements of the nanocomposites properties.

Organophilization via cation exchange for both hydrated fillers, natural MMT and Mg-hect, involves both external and internal surfaces. The organophilized nanofillers were termed as O/MMT and O/Mg-hect. The complete exchange can be indicated by a shift in the basal spacing from 13.5 to 17.4 Å and from 14.6 to 18.2 Å for O/MMT and O/Mg-hect, respectively (Fig. 2). Complete exchange of inorganic interlayer cations in both O/MMT and O/Mg-hect reduces the attractive Coulomb forces between the silicate layers and thus the shear strength in the tactoid is decreased.

Contrary to the hydrated fillers (O/MMT and O/Mg-hect), due to the inertness of the interlayer in the shear-

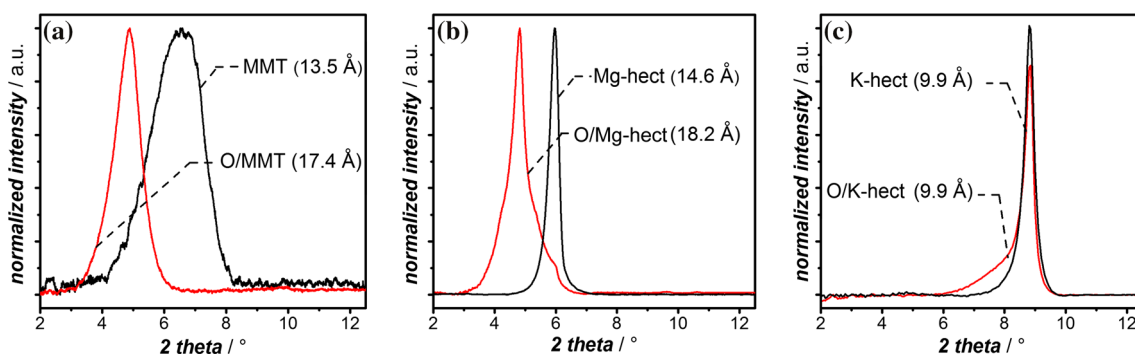


**Fig. 2** PXRD patterns of the basal reflection ( $d(001)$ ) of the employed nanofillers before and after organophilization

stiff K-hect, the modification is restricted to the external basal surfaces. The organophilized K-hect (O/K-hect) consequently shows no shift in the basal spacing (9.9 Å) which is typical for non-hydrated 2:1 layered silicates (Fig. 2c). This theoretically higher shear stiffness state is expected to minimize any possible gliding of adjacent layers, perpendicular to stacking direction under shear loading [23].

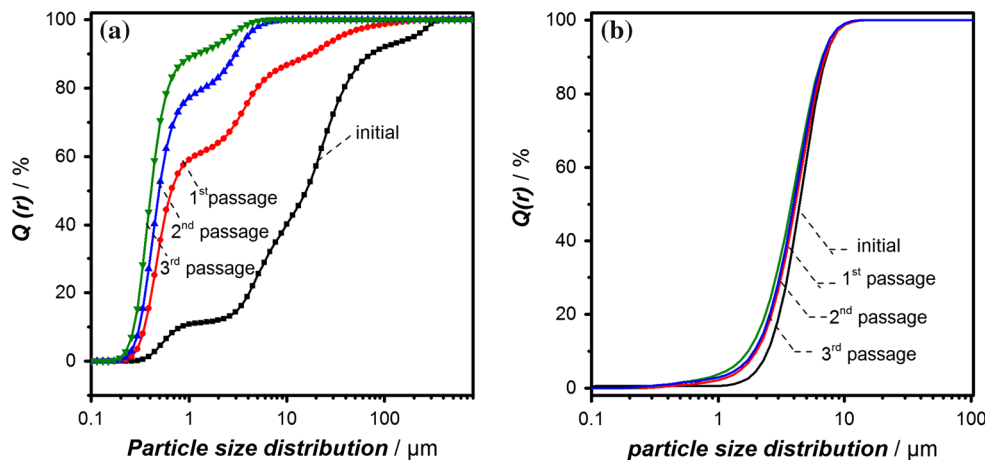
Furthermore, the amount of organic content of the three different organophilized nanofillers was determined by TGA measurements. It was found to be 4.4, 16.7, and 15.8 wt% for O/K-hect, O/Mg-hect, and O/MMT, respectively. The observed significant difference is another consequence of the diverging intracrystalline reactivity of the different nanofillers. Considering the amount of organic content, the densities of the organophilized nanofillers were determined to  $2.1 \text{ g cm}^{-3}$  for both O/MMT and O/Mg-hect and  $2.7 \text{ g cm}^{-3}$  O/K-hect. These densities are used to determine the filler content by volume.

### Morphology and dispersion quality

Minimizing any possible aggregation and hence maximizing the specific interface between matrix and nanofiller is a

prerequisite for an optimized performance of nanocomposites. In order to analyze the effect of particle size it is necessary to monitor the lateral extension of the different nanofillers during nanocomposite preparation. Changes in the particle size distribution during the dispersion process in the three roll mill may serve as a first indication of the degree of aggregation and were therefore monitored applying SLS. Prior to three roll milling, huge aggregates were determined for O/MMT indicated by a multimodal distribution (Fig. 3a). No detectable amounts of primary platelets smaller than 350 nm could be observed. With increasing numbers of milling passages applied, a continuing disaggregation occurs, yielding to smaller particle sizes and a narrower distribution. However, a complete disaggregation of O/MMT could not be achieved since some aggregates are detected after the third passage. This can be attributed to the iron- and aluminum-oxihydroxides impurities associated with natural MMT deposits. On the contrary, no aggregates were detected by SLS measurements for the O/Mg-hect suspension before processing in the three roll mill. Moreover, no significant breakage of the large particles occurs during processing (Fig. 3b). The same is true for the shear-stiff O/K-hect where again, upon processing, no significant changes in the particle size

**Fig. 3** Evolution of cumulative, volume-weighted particle size distributions obtained by SLS for **a** O/MMT and **b** O/Mg-hect in THF suspension during processing in the three roll mill with respect to the number of applied passages



distribution were observed. These results highlight the efficiency of the chosen dispersing method to achieve the required homogenization and disaggregation of the nanofillers in the matrix while avoiding breakage of the nanoplatelets.

Following the curing of the epoxy/clay nanocomposites, PXRD patterns were obtained to monitor any possible changes in basal spacing due to (partial) intercalation (Fig. 4). Despite the significant dilution of the filler in the matrix, leading to peak intensities, the basal spacings are still clearly detectable and no shifts of the basal reflections occurred during dispersion and curing (compare Fig. 2). Consequently no additional swelling respectively intercalation of all three types of organophilized nanofiller occurred during dispersion and curing. Additionally, the PXRD results reveal a random particle distribution in the nanocomposite powders since the basal reflection intensities are not enhanced as compared to the textured clay films obtained in reflection mode (Fig. 2).

TEM permits a qualitative observation of the internal structure of the nanocomposites through direct visualization of the filler distribution in the matrix. Figure 5 shows TEM micrographs of the nanocomposites at the highest nanofiller content. For O/MMT-filled nanocomposites (Fig. 5a), the processing technique yielded a homogenous dispersion of mostly single O/MMT tactoids. Nevertheless, as expected from SLS observations, few micro-aggregates with an average particle size larger than 2  $\mu\text{m}$  were identified. The presence of such aggregates reduces the specific interface area significantly and consequently is expected to be detrimental for the final nanocomposites properties.

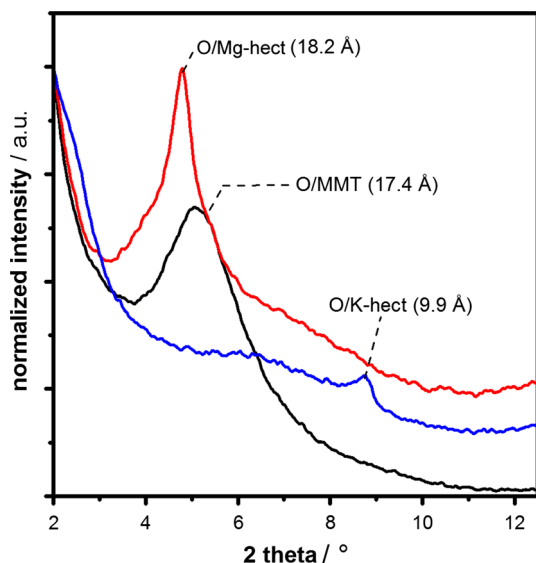


**Fig. 4** PXRD patterns of the different ground epoxy/clay nanocomposites measured in transmission geometry

For O/Mg-hect- and O/K-hect-filled nanocomposites (Fig. 5b, c), homogeneously dispersed individual tactoids were observed. Since the preparation process excluded any drying steps, the formation of band-like structure aggregates was avoided even for such large nanoplatelets.

### Thermo-mechanical properties

Dynamic mechanical thermal analysis (DMTA) was used to characterize the relaxation properties of the different nanocomposites related to the type and content of the nanofiller. It was seen that the glass transition temperatures ( $T_g$ ) of the nanocomposites were reduced with increasing the nanofiller content (Fig. 6). Comparing the influence of the different nanofillers, the decrease in  $T_g$  of the nanocomposites filled with the small O/MMT was the most pronounced. At the highest filler content (2.8 vol%), the addition of O/MMT provoked a drop in  $T_g$  by 20  $^{\circ}\text{C}$ , whereas the  $T_g$  of nanocomposites filled with the larger O/Mg-hect and O/K-hect was less influenced by the filler content. At the highest content of O/Mg-hect (2.8 vol%), a decrease in  $T_g$  of only 11  $^{\circ}\text{C}$  was observed.

Comparable tendencies were revealed in similar studies based on epoxy resins filled with organically modified clays [5, 15, 24]. As an example, the  $T_g$  of an epoxy nanocomposite filled with 5 wt% synthetic fluorohectorite (Somasilf ME 100) modified with dodecyl ammonium was reduced from 133 to 116  $^{\circ}\text{C}$  [5]. As described by Messersmith and Giannelis [25], the observed changes in the glass transition temperature are related to the molecular mobility of polymer chain segments at the polymer/nanofiller interface. Consequently, the changes are strongly dependent on both the quality of the interfacial interaction and specific surface area [5, 26, 27]. In the present study, the aliphatic dodecyl tail of the surface modifier is too short to achieve any entanglements, and it is not capable to form covalent cross-links with the thermosetting matrix during curing. Therefore, a moderate interaction between the polymer matrix and the nanofillers is assumed. Due to the moderate interaction, the dodecyl chains may act as steric spacers inducing a higher dynamic of the polymer network around the filler. This consequently increases the molecular dynamics of the polymer network locally at the interface, leading to diminishing of the main transition relaxation times of the affected polymer network. As a result, an overall drop of  $T_g$  is observed.

In order to analyze the influence of the particle geometry on the glass transition temperature, the number of nanoparticles,  $n_{\phi}$ , in a reference volume  $V_c$  is calculated with respect to the filler content,  $\phi$ , according to Eq. (5), where  $\bar{V}_{np}$  the volume of the nanoplatelets (mean value) calculated from the mean tactoid height,  $\bar{h}_{\text{clay}}$  and the mean clay

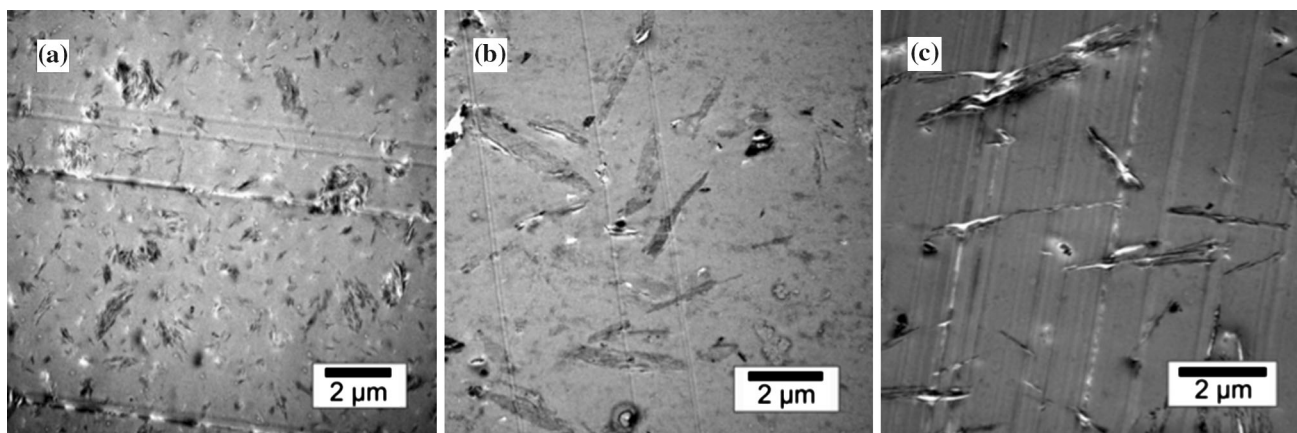


**Fig. 5** TEM micrographs of epoxy/clay nanocomposites at the highest nanofiller content for **a** O/MMT, **b** O/Mg-hect, and **c** O/K-hect

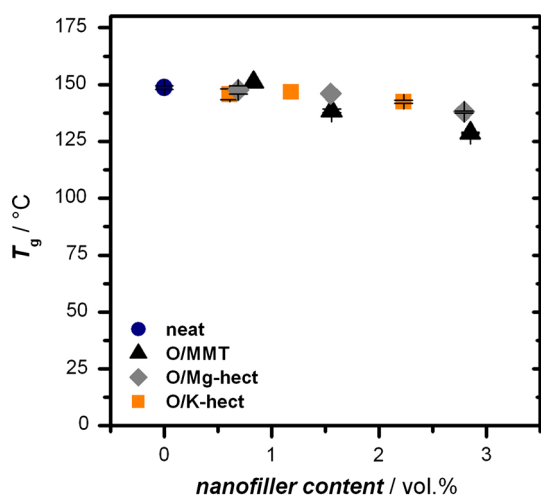


**Fig. 6** Glass transition temperature of the epoxy/clay nanocomposites with respect to nanofiller type and content, assessed from  $\tan \delta$  maximum by dynamic mechanical thermal analysis

diameter,  $\bar{d}_{\text{clay}}$ . As a mean value of  $\bar{h}_{\text{clay}}$ , a value of ten times the intergallery distance is estimated. For all estimations, the nanoplatelets were approximated as cylinders.

$$n_{\phi} = \phi_f \cdot \frac{V_c}{V_{\text{np}}} = \phi_f \cdot \frac{4 \cdot V_c}{\pi \cdot \bar{h}_{\text{clay}} \cdot \bar{d}_{\text{clay}}^2} \quad (5)$$

At any given volume fraction, the number of O/MMT particles is at least two orders of magnitude higher as the number of the large synthetic fluorohectorites particles. This fact is exemplarily shown for  $V_c = 1 \text{ cm}^3$  and  $\phi = 2.7 \text{ vol}\%$  in Table 3.

Furthermore, the surface area of the three types of nanofillers is calculated according to Eq. (6). In the calculation of the surface area, the lateral surface is neglected since the front surface is more relevant for particle matrix interactions [28].

$$\bar{S}_{\text{clay},\phi} = \frac{\pi \cdot \bar{d}_{\text{clay}}^2}{2} \quad (6)$$

As expected the mean surface area of the small MMT particles is lower as compared to the larger synthetic fluorohectorites (Table 3). O/Mg-hect and O/K-hect have the same surface area since these particles just differ in the intergallery distance. However, in correlation with the number of particles, the total surface area of all three types of nanofillers is comparable. Consequently the drop in  $T_g$  might not be related to different surface areas.

In order to deepen our understanding on the influence of the nano-particle geometry on  $T_g$  and the molecular mobility, the affected volume in the vicinity of the nano-particles (Fig. 7) was estimated considering the different particle geometries. To simplify the rough estimation of the

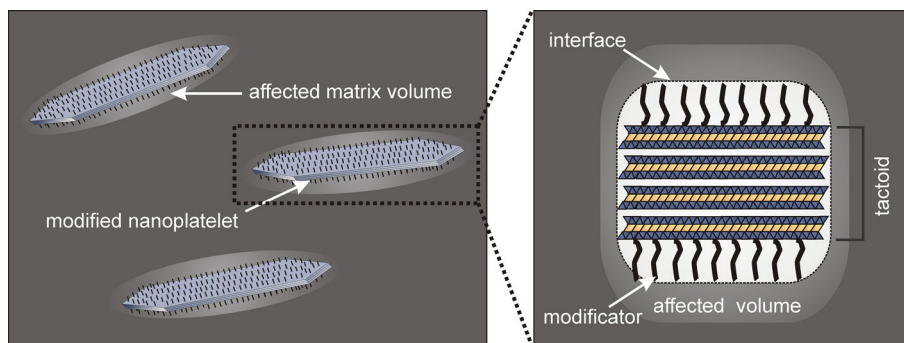
**Table 3** Estimated number of nanoplatelets, surface area, and affected volume for the different types of nanofillers

Type of nanofiller	Number of particles <sup>a</sup>	Mean surface per nano-particle (m <sup>2</sup> )	Affect volume/particle volume	Mean affected volume per nano-particle (cm <sup>3</sup> )	Total affected volume <sup>a</sup> (cm <sup>3</sup> )
O/MMT	$1.1 \times 10^{13}$	$2.5 \times 10^{-13}$	1.205	$3.03 \times 10^{-15}$	0.0325
O/Mg-hect	$1.4 \times 10^{11}$	$1.9 \times 10^{-11}$	1.023	$1.97 \times 10^{-13}$	0.0276
O/K-hect	$2.8 \times 10^{11}$	$1.9 \times 10^{-11}$	1.011	$9.73 \times 10^{-14}$	0.0273

<sup>a</sup> In  $1 \text{ cm}^3$  at a filler content of 2.7 vol%



**Fig. 7** Schematic representation of the affected polymer matrix volume at the interface between the nanofiller and the cured epoxy matrix



affected volume, it was assumed that the affected volume surrounding the nanoplatelets has a homogenous finite thickness of  $0.5 \bar{h}_{\text{clay}}$ . To estimate the thickness of the affected volume more precisely, small angle scattering experiments (SAXS and SANS) should be considered, which do not fall within the aim of this publication. However, this will effectively be a very promising perspective for this work. In Table 3, the ratio of the affected volume to the particle volume is given for the three different types of clay. It is obvious that this ratio is the highest for the small O/MMT nanoplatelets. The higher amount of affected polymer network respectively interfacial volume is resulting in intensified molecular dynamics in the periphery of the polymer/nanofiller interface. Hence the highest decrease in  $T_g$  for the O/MMT nanocomposites observed is plausible.

**Mechanical properties**

*Tensile properties*

Tensile properties for different epoxy/clay nanocomposites were determined with respect to the type and volume content of the nanofiller (Figs. 8, 9, 10). As expected, the incorporation of nanoclays led to a significant increase in the Young’s moduli as a function of nanofiller content since the clay nanoplatelets possess higher moduli than the neat epoxy matrix. The presence of the nanoplatelets significantly restricts the mechanical mobility of the polymer network globally. This effect is more pronounced at higher filler contents since the interaction of the stress fields around the nano-particles, respectively, the formation of a continuous interphase becomes more probable.

At a given volume content, the aspect ratio is the key factor influencing the nanocomposite stiffness as expressed by the Halpin–Tsai equation [29]. The synthetic nanofillers (O/Mg-hect and O/K-hect) have significantly higher aspect ratio (up to 430, respectively, 860) as compared to the natural O/MMT nanofiller (up to 35). This leads to higher moduli at lower volume fraction (Fig. 8). It is noteworthy

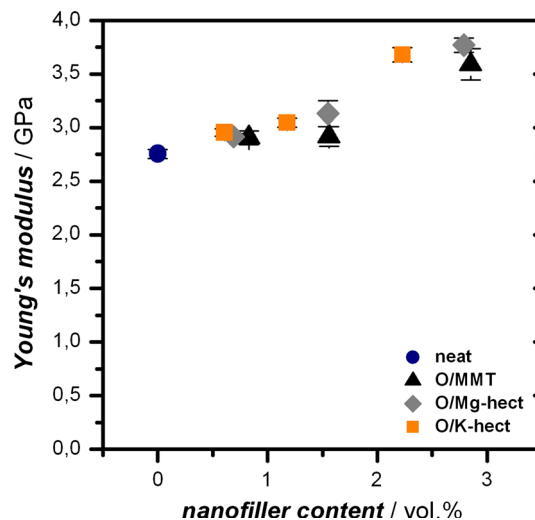


**Fig. 8** Young’s modulus of the different epoxy/clay nanocomposites with respect to the nanofiller content

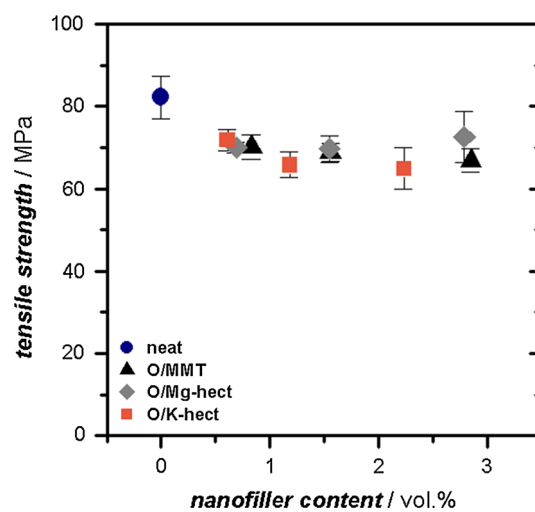


**Fig. 9** Tensile strength of the different epoxy/clay nanocomposites with respect to the nanofiller content

to mention that both O/Mg-hect and O/K-hect have the same lateral extension but two different interlayer distances, consequently, they differ in the tactoid height ( $h$ ) as

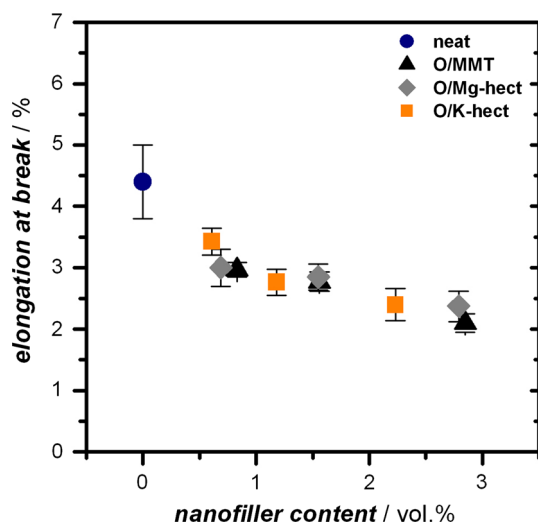


**Fig. 10** Elongation at break of the different epoxy/clay nanocomposites with respect to the nanofiller content

shown in Fig. 2. Therefore, O/Mg-hect has a lower aspect ratio as compared to O/K-hect. Accordingly, the most significant improvement in the Young's modulus was observed for the O/K-hect filled epoxy nanocomposites due to the highest aspect ratio. Furthermore, the higher shear stiffness of the tactoids has a favorable influence.

The increase in Young's Modulus is achieved nevertheless at the expense of tensile strength (Fig. 9) and elongation at break (Fig. 10). Similar observations for a decrease in tensile strength and elongation at break were reported in literature [5, 15, 30]. For instance, incorporation of organophilized hectorite (Somafix ME 100) in an epoxy matrix reduced the tensile strength significantly even at low volume fraction [5]. This reduction was attributed to various phenomena including micron size agglomerates [5, 15], heterogeneous network density [30], or a weak epoxy/clay interface adhesion [31].

As seen in the TEM micrographs (Fig. 5), the prepared samples show little to no aggregates due to the optimized dispersing technique. Furthermore, a slight change in the network density in the vicinity of the nanofiller is expected due to moderate interaction between the nanofiller and the matrix. In this case, the decrease in tensile strength is most probably related to stress concentration at the sharp tactoid edges resulting in flaws within the interface. These stress concentrations are more pronounced for large synthetic O/K-hect characterized by a collapsed structure, due to the thinner tactoids. Surprisingly, the large primary nanoplatelets did not provoke any further detrimental effect on tensile strength and elongation at break in comparison to the other types of nanofillers.

In order to confirm the assumptions of Kinloch and Taylor [7], the Poisson ratio,  $\nu$ , was determined. As

expected a value of  $\nu = 0.35$  was found, within the limits of accuracy, independently from type and content of nanofiller.

### Fracture toughness

Linear elastic fracture mechanics were employed to evaluate the impact of the three different nanofillers on the fracture toughness in terms of the critical stress intensity factor,  $K_{Ic}$  (Fig. 11). Especially the influence of particle size (lateral extension) and stiffness state is discussed.

The brittle behavior of the neat epoxy is reflected in the low  $K_{Ic}$  value of  $0.47 \text{ MPa m}^{0.5}$ . The incorporation of all three different nanofillers led to an improved fracture toughness in relation to the nanofiller content. The addition of 2.8 vol% O/MMT (small lateral extension) results in an increase up to  $0.69 \text{ MPa m}^{0.5}$  (47 %). Moreover, a more pronounced enhancement of 68 % ( $0.79 \text{ MPa m}^{0.5}$ ) is measured for the larger O/Mg-hect nanoplatelets at the same volume fraction. As anticipated, the large but shear-stiff nanoplatelets of O/K-hect lead to the most prominent improvement of  $0.84 \text{ MPa m}^{0.5}$  (78 %) even at 2.2 vol%. Obviously a higher toughening effect is related to the size of the dispersed nanofiller. The large lateral extension of fluorohectorite nanoplatelets (O/Mg-hect and O/K-hect) contributed to a more pronounced toughening effect as compared to the much smaller O/MMT nanoplatelets. Alongside the particle size, the stiffness of the nanofiller is a key factor influencing the fracture toughness. The higher shear stiffness, as for O/K-hect, increases the load bearing ability in the layer stacking direction and the flexural rigidity of the tactoids. This is due to the presence of the non-hydrated  $K^+$ -ions in the interlayer distance bridging the layers [16]. Further investigation of the occurring

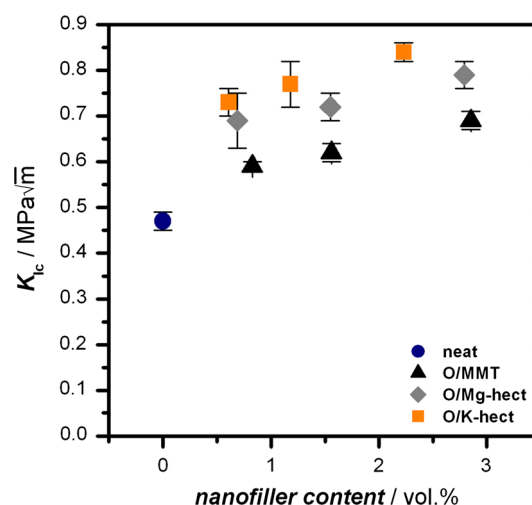


**Fig. 11**  $K_{Ic}$  of the different epoxy/clay nanocomposites with respect to the nanofiller content

energy dissipating mechanisms and their relation to the particle size and stiffness state is addressed hereafter.

### Toughening mechanisms

The occurring toughening mechanisms during mode I crack propagation were deduced from the morphology of fracture surfaces (CT-specimen) using scanning electron microscopy (Fig. 12). All micrographs were taken from the center of the sample in the vicinity of the notched region.

As it is typical for neat epoxies, the fracture surface is smooth, showing no obvious plastic deformation during crack propagation (Fig. 12a). On the contrary, the fracture surfaces of the epoxy/clay nanocomposites reveal more tortuous crack propagation paths depending on the lateral extension and stiffness state of the used nanofiller (Fig. 12b, c, d). The fracture surfaces of O/MMT-filled nanocomposites are characterized by a rough structure exhibiting a large number of voids (Fig. 13a) initiated from particle debonding (Fig. 13b). As a consequence, particle debonding followed by void formation and growth by shear yielding of the matrix were identified as the main occurring toughening mechanisms.

However, from the fracture surfaces of the nanocomposites filled with the large synthetic fluorohectorite

nanoplatelets (up to 8  $\mu\text{m}$ ), further toughening mechanisms like crack deflection and crack pinning were identified (Fig. 12c, d). The large lateral extensions of the nanoplatelets led to additional energy dissipation by a local crack deflection since the crack is forced to propagate along the interface between the epoxy resin and the clay nanoplatelets. As a consequence of the interfacial crack growth, debonding of the nanoplatelets was observed at higher magnification. The surface of the debonded platelets is smooth, which confirms the assumed moderate adhesion between the nanofiller and the epoxy matrix (Fig. 14).

The investigation of the fracture surfaces of the O/Mg-hect-filled nanocomposites reveals the occurrence of similar toughening mechanisms (Fig. 15). The  $K_{Ic}$  values were lower as compared to the O/K-hect-filled nanocomposites. Interestingly, SEM micrographs show the cleavage of the shear-labile tactoids during crack propagation, which might be an explanation for the lower fracture toughness.

### Micromechanics

The impact of particle size on toughening mechanisms is further analyzed by a fracture mechanics approach. During crack propagation, plastic yielding of the matrix occurs in the plastic zone at the very close region of the crack tip.

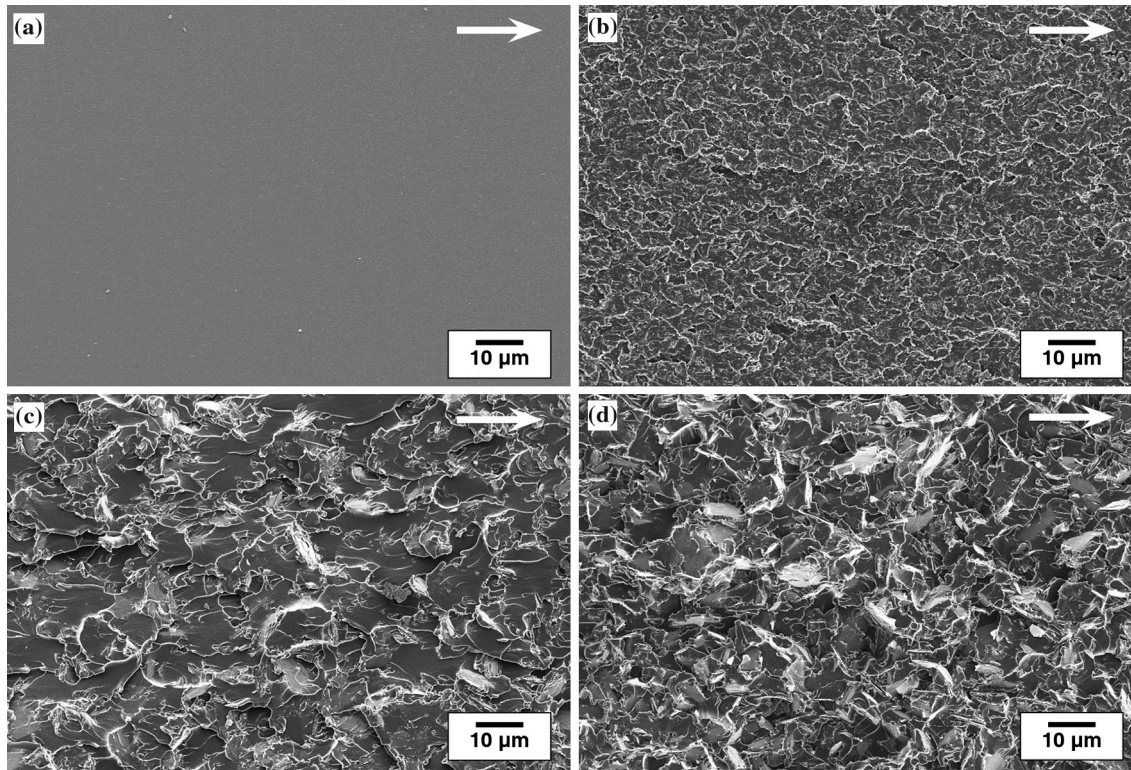


**Fig. 12** SEM micrographs of fracture surfaces of **a** neat epoxy, and the different nanocomposites filled with **b** O/MMT (2.8 vol%), **c** O/Mg-hect (2.8 vol%), and **d** O/K-hect (2.2 vol%). The direction of crack propagation is from *left to right* as indicated by the *arrows*

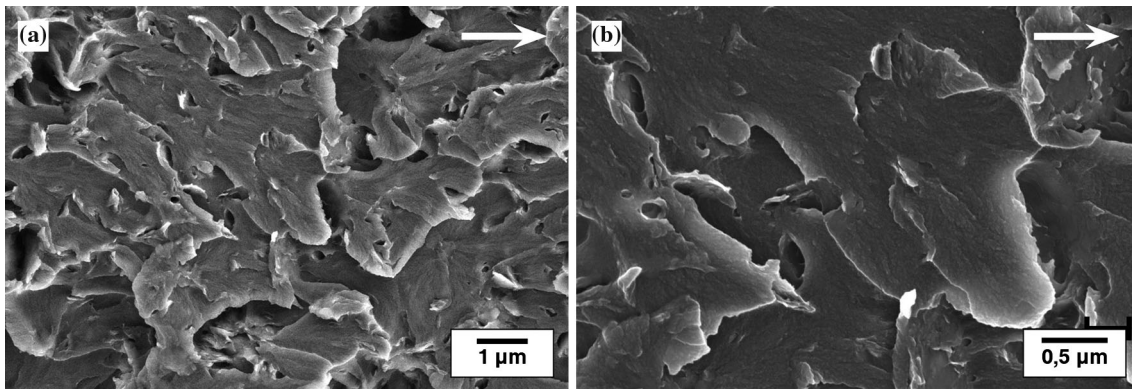


**Fig. 13** SEM micrographs of fracture surfaces of O/MMT epoxy nanocomposite (2.8 vol%) at higher magnification revealing void formation and growth. The direction of crack propagation is from *left to right* as indicated by the *arrows*

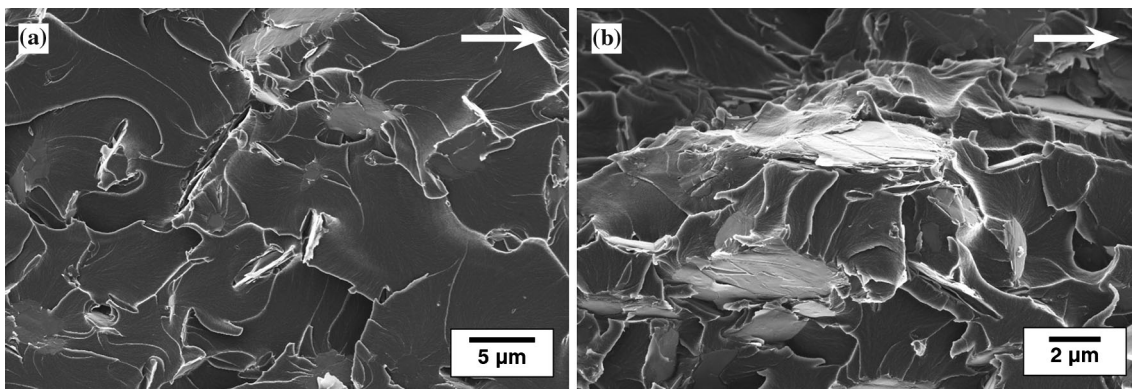


**Fig. 14** SEM micrographs at higher magnification of O/K-lect-filled nanocomposite **a** at 0.6 vol% showing crack pinning and crack deflection and **b** the smooth debonded nanofiller surface is pointed

out (2.2 vol%). The direction of crack propagation is from *left to right* as indicated by the *arrows*

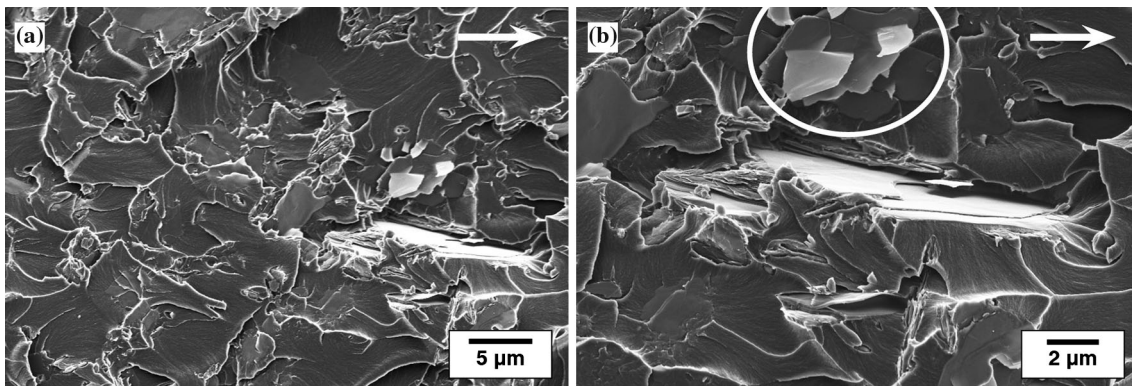


**Fig. 15** Higher magnification SEM micrographs of O/Mg-lect-filled nanocomposite (2.8 vol%) **a** showing crack pinning and crack deflection, and **b** the smooth debonded nanofillers surface. The

highlighted area shows the cleavage of a shear-labile tactoid. The direction of crack propagation is from *left to right* as indicated by the *arrows*

The presence of nano-particles might influence the shape of the plastic zone. Nevertheless, a cylindrical plastic zone is considered as a first approximation. The diameter of the plastic zone for the epoxy/clay nanocomposites (Table 4)

was calculated from Irwin's analysis (Eq. 3). Obviously, the fluorohectorite nanoplatelets characterized by large lateral extensions (up to 8.6 μm) are in the same order of magnitude as the plastic zone diameter. Hence, the plastic

**Table 4** Diameter of the plastic zone and crack tip opening displacement ( $\delta_{tc}$ ) in epoxy/clay nanocomposites

Type of nanofiller	Nanofiller content (wt%/vol%)	Diameter of plastic zone ( $\mu\text{m}$ )	Crack tip opening displacement ( $\delta_{tc}$ ) ( $\mu\text{m}$ )
Unfilled	0	$3.5 \pm 0.7$	$0.9 \pm 0.1$
O/MMT	1.5/0.8	$5.5 \pm 0.9$	$1.3 \pm 0.1$
	2.8/1.6	$6.0 \pm 1.1$	$1.4 \pm 0.2$
	5.0/2.8	$7.5 \pm 1.4$	$1.4 \pm 0.2$
O/Mg-hect	1.4/0.6	$7.5 \pm 2.2$	$1.7 \pm 0.4$
	2.7/1.2	$8.1 \pm 1.7$	$1.8 \pm 0.3$
	5.0/2.2	$9.8 \pm 1.4$	$1.8 \pm 0.2$
O/K-hect	1.2/0.7	$8.4 \pm 1.7$	$1.9 \pm 0.3$
	2.8/1.6	$9.3 \pm 3.4$	$2.1 \pm 0.4$
	4.9/2.8	$11.1 \pm 1.9$	$2.0 \pm 0.2$

zone is almost fully spanned by a single tactoid and consequently crack propagation is highly constrained. In contrast, the size of the O/MMT particles is as small as the diameter of the plastic zone and hence the direction of the crack propagation is less influenced.

In order to understand the occurring toughening mechanisms the average particle size is compared to the crack tip opening displacement ( $\delta_{tc}$ ), as calculated from Eq. (4). The resultant values are given in Table 4. The sharpness of the crack tip, reflected in  $\delta_{tc}$ , is altered by the plastic yielding of the matrix in the vicinity of the crack tip. However, to promote effective toughening mechanisms, in particular crack pinning and crack deflection, the filler must be at least as large as  $\delta_{tc}$  [32, 33]. The  $\delta_{tc}$  of O/MMT-filled nanocomposites ( $\approx 1.4 \mu\text{m}$ ) is approximately twice the maximum particle size of MMT ( $\approx 750 \text{ nm}$ ). Consequently, crack deflection and crack pinning are unlikely to occur since the particles are too small for effective crack tip/particle interactions. On the contrary, the  $\delta_{tc}$  values for O/Mg-hect- and O/K-hect-filled nanocomposites (1.7 to  $2.1 \mu\text{m}$ ) are below the average lateral extensions of these nanofillers ( $\approx 3.8 \mu\text{m}$ ) allowing the aforementioned toughening mechanisms to occur as it was revealed by SEM investigations.

*Energy release rate*

The energy release rate ( $G_{Ic}$ ) of the nanocomposites was calculated using Eq. (2) by relating the stress intensity factor (Fig. 10) and the Young’s modulus determined by tensile testing (Fig. 8). The addition of all three different types of nanofillers led to an increase in  $G_{Ic}$ , although no continuous enhancement with increasing filler content was observed. Moreover, above a filler content of as low as 1 vol%, already a plateau was reached and the  $G_{Ic}$  does not increase further within the experimental errors at higher

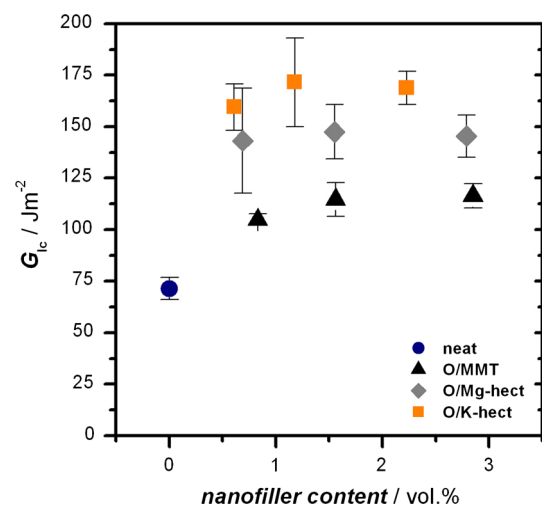


**Fig. 16**  $G_{Ic}$  of the different epoxy/clay nanocomposites with respect to the nanofiller content

filler loadings (Fig. 16). For the shear-labile O/MMT-filled epoxy nanocomposites having  $0.4 \mu\text{m}$  lateral extension, the maximum value for  $G_{Ic}$  was  $116 \text{ Jm}^{-2}$ , which is equivalent to an increase of 62 % as compared to the neat epoxy matrix ( $71 \text{ Jm}^{-2}$ ). The larger shear-labile O/Mg-hect nanoplatelets ( $\approx 3.8 \mu\text{m}$ ) led to a more pronounced increase of up to  $147 \text{ Jm}^{-2}$  (106 %). Notably, the highest increase in  $G_{Ic}$  of up to  $171 \text{ Jm}^{-2}$  (140 %) was obtained for the nanocomposites filled with the large ( $\approx 3.8 \mu\text{m}$ ) and shear-stiff O/K-hect.

Considering Eq. (2), the observed trend in  $G_{Ic}$  with increasing nanofiller content is a consequence of the progressive increase in Young’s modulus and the respective non-proportional increase in  $K_{Ic}$ . The occurrence of a maximum in  $G_{Ic}$  at a certain filler content was already reported by Zilg et al. [5]. Zerda and Lesser [34] postulated that this maximum occurs due to a critical interparticle

distance. According to Kinloch and Taylor [7], the interparticle distance strongly affects the energy release rate, although no critical value could be identified. At high filler contents, the interparticle distance is reduced which is followed by an increase of stress field interactions around the nano-particles. These stress field interactions cause the observed progressive increase in Young's Modulus since the restriction of the matrix mobility is intensified. However, these stress field interactions might reduce the efficiency of a single particle in terms of toughening.

In the case of O/MMT nanocomposites, toughening is dominated by particle debonding and subsequent void growth accompanied with plastic flow of the matrix. As a consequence of the reduced interparticle distance at higher nanofiller contents, the probability of void coalescence is increased resulting in accelerated crack propagation respectively a less pronounced  $K_{Ic}$  increase. Concerning the O/Mg- and O/K- filled nanocomposites, the role of the interparticle distance is different since crack deflection is the major toughening mechanism. In case of stress field interactions at reduced interparticle distances, the crack is deflected on these stress fields assemblies of closely located nanofillers rather than individual nanoplatelets. The presence of such assemblies might diminish the toughening effect of single dispersed tactoids above the critical filler content. As a consequence, the non-linear increase in  $K_{Ic}$  at higher filler contents is observed. Relating these facts with the increasing Young's modulus with respect to the number of nano-particles, the observed trend in  $G_{Ic}$  values is reasonable.

## Conclusion

In this work, the improved fracture toughness of epoxy layered silicates nanocomposites is related to the dispersed reinforcing nanofiller, in terms of particle size (lateral extension) and mechanical properties (stiffness state). In order to maximize the specific interface area in the nanocomposites, a combination of solution blending and a three roll mill process is applied.

A significantly higher increase in fracture toughness is observed for the large synthetic O/Mg- as compared to common MMT (O/MMT). This is due to the large lateral extension of such synthetic nanoplatelets (up to 8  $\mu\text{m}$ ) which contributes to effective energy dissipation mechanisms such as crack deflection. Moreover, the absence of such toughening mechanisms for O/MMT-filled nanocomposites is explained due to the fact that their mean particle size (400 nm) is much smaller than the crack tip opening displacement.

Further improvement in fracture toughness is achieved using the shear-stiff O/K-. For this material

interlamellar crack propagation and/or particle cleavage is impeded due to the collapsed tactoid structure. In summary, the shear-stiff O/K- is an outstanding type of nanofiller for the preparation of epoxy nanocomposites. These nanocomposites provide a subtle balance between high stiffness and high fracture toughness even at very low content (0.6 vol%).

**Acknowledgements** The authors highly acknowledge the financial support from the German Research Foundation in the frame of the Collaborative Research Center SFB 840: "From particulate nanosystems to mesotechnology," and from the German Federal Ministry for Economic Affairs and Energy (FKZ 0327895E).

## References

- Levita G, De Petris S, Marchetti A, Lazzeri A (1991) Crosslink density and fracture toughness of epoxy resins. *J Mater Sci* 26:2348–2352. doi:10.1007/BF01130180
- Sprenger S (2013) Epoxy resins modified with elastomers and surface-modified silica nanoparticles. *Polymer* 54:4790–4797
- Sprenger S, Kothmann MH, Altstädt V (2014) Carbon fiber-reinforced composites by modifying the epoxy resin with reactive liquid rubber and silica nanoparticles. *Compos Sci Technol* 105:86–95
- Kothmann MH, Zeiler R, Rios de Anda A, Brückner A, Altstädt V (2015) Fatigue crack propagation behaviour of epoxy resins modified with silica-nanoparticles. *Polymer* 60:157–163
- Zilg C, Mühlhaupt R, Finter J (1999) Morphology and toughness/stiffness balance of nanocomposites based upon anhydride-cured epoxy resins and layered silicates. *Macromol Chem Phys* 200:661–670
- Becker O, Varley RJ, Simon GP (2002) Morphology, thermal relaxations and mechanical properties of layered silicate nanocomposites based upon high-functionality epoxy resins. *Polymer* 43:4365–4373
- Kinloch AJ, Taylor AC (2006) The mechanical properties and fracture behaviour of epoxy-inorganic micro- and nano-composites. *J Mater Sci* 41:3271–3297. doi:10.1007/s10853-005-5472-0
- Dzenis Y (2008) Structural nanocomposites. *Science* 319:419–420
- Fischer S, Salcher A, Kornowski A, Weller H, Förster S (2011) Completely miscible nanocomposites. *Angew Chem Int Ed* 50:7811–7814
- Paul DR, Robeson LM (2008) Polymer nanotechnology: nanocomposites. *Polymer* 49:3187–3204
- Mittal V (2012) Modification of montmorillonites with thermally stable phosphonium cations and comparison with alkylammonium montmorillonites. *Appl Clay Sci* 56:103–109
- Becker O, Cheng Y-B, Varley RJ, Simon GP (2003) Layered silicate nanocomposites based on various high-functionality epoxy resins: the influence of cure temperature on morphology, mechanical properties, and free volume. *Macromolecules* 36:1616–1625
- Köster HM (1996) Mineralogical and chemical heterogeneity of three standard clay mineral samples. *Clay Miner* 31:417–422
- Breu J, Range KJ, Kohler EE, Wagner U (1993) Oxidation state of iron at the interface of composite basal lining systems. *Appl Clay Sci* 8:313–320
- Korrmann X, Thomann R, Mühlhaupt R, Finter J, Berglund L (2002) Synthesis of amine-cured, epoxy-layered silicate nanocomposites: the influence of the silicate surface modification on the properties. *J Appl Polym Sci* 86:2643–2652

16. Möller MW, Handge UA, Kunz DA, Lunkenbein T, Altstädt V, Breu J (2010) Tailoring shear-stiff, mica-like nanoplatelets. *ACS Nano* 4:717–724
17. Kalo H, Möller MW, Kunza DA, Breu J (2012) How to maximize the aspect ratio of clay nanoplatelets. *Nanoscale* 4:5633–5639
18. Ziadeh M, Chwalka B, Kalo H, Schütz MR, Breu J (2012) A simple approach for producing high aspect ratio fluorohectorite nanoplatelets utilizing a stirred media mill (ball mill). *Clay Miner* 47:341–353
19. Ammann L, Bergaya F, Lagaly G (2005) Determination of the cation exchange capacity of clays with copper complexes revisited. *Clay Miner* 40:441–453
20. Goossens D (2008) Techniques to measure grain-size distributions of loamy sediments: a comparative study of ten instruments for wet analysis. *Sedimentology* 55:65–96
21. KA Carrado, A Decarreau, S Petit, F Bergaya, G Lagaly (2006) Synthetic clay minerals and purification of natural clay. In: *Handbook of clay science* Bergaya F, Theng BKG, Lagaly G (eds), Chapter 4, 1st edn. Elsevier, Amsterdam
22. Kinloch AJ, Young RJ (1983) *Fracture behaviour of polymers*. Applied Science Publishers, London
23. Sheng N, Boyce MC, Parks DM, Rutledge GC, Abes JI, Cohen RE (2004) Multiscale micromechanical modeling of polymer/clay nanocomposites and the effective clay particle. *Polymer* 45:487–506
24. Liu T, Tjiu WC, Tong Y, He C, Goh SS, Chung T-S (2004) Morphology and fracture behavior of intercalated epoxy/clay nanocomposites. *J Appl Polym Sci* 94:1236–1244
25. Messersmith PB, Giannelis EP (1994) Synthesis and characterization of layered silicate-epoxy nanocomposites. *Chem Mater* 6:1719–1725
26. Zilg C, Thomann R, Finter J, Mülhaupt R (2000) The influence of silicate modification and compatibilizers on mechanical properties and morphology of anhydride-cured epoxy nanocomposites. *Macromol Mater Eng* 280–281:41–46
27. Mouloud A, Cherif R, Fellahi S, Grohens Y, Pillin I (2012) Study of morphological and mechanical performance of amine-cured glassy epoxy–clay nanocomposites. *J Appl Polym Sci* 124: 4729–4739
28. Shi H, Lan T, Pinnavaia TJ (1996) Interfacial effects on the reinforcement properties of polymer–organoclay nanocomposites. *Chem Mater* 8:1584–1587
29. Yung KC, Wang J, Yue TM (2006) Modeling young’s modulus of polymer-layered silicate nanocomposites using a modified halpin-tsai micromechanical model. *J Reinf Plast Compos* 25:847–861
30. Wang K, Chen L, Wu J, Toh ML, He C, Yee AF (2005) Epoxy nanocomposites with highly exfoliated clay: mechanical properties and fracture mechanisms. *Macromolecules* 38:788–800
31. Fu S-Y, Feng X-Q, Lauke B, Mai Y-W (2008) Effects of particle size, particle/matrix interface adhesion and particle loading on mechanical properties of particulate–polymer composites. *Compos B Eng* 39:933–961
32. Johnsen BB, Kinloch AJ, Mohammed RD, Taylor AC, Sprenger S (2007) Toughening mechanisms of nanoparticle-modified epoxy polymers. *Polymer* 48:530–541
33. Ziadeh M, Fischer B, Schmid J, Altstädt V, Breu J (2014) On the importance of specific interface area in clay nanocomposites of pmma filled with synthetic nano-mica. *Polymer* 55:3770–3781
34. Zerda AS, Lesser AJ (2001) Intercalated clay nanocomposites: morphology, mechanics, and fracture behavior. *J Polym Sci B* 39:1137–1146